Memoirs of the School of Engineering, Nagoya University
Vol.44. No.2 (1992) − Research Report −

NUMERICAL ANALYSIS OF INTERACTION OF SUPERSONIC FREE JETS, INCLUDING FORMATION OF REVERSE FLOW

Takeo SOGA and Takehiko HAYASHI*

Department of Aeronautical Engineering

(Received November 12, 1992)

Abstract

Interaction of free jets from multi-orificies was studied within the frame work of Euler equation. The Piecewise Linear Method was employed as the Euler solver where free jets were issued from square sonic orifices. Impingement of supersonic free jets from two orifices yielded (almost) plane oblique shock waves. Compressed and heated gas behind these shock waves resulted in an intensive secondary jet, which merged into the primary jets. The primary cells of free jets were consequently enlarged. In the case of free jets from four orifices the secondary jet was so intensive that each primary cell was isolated by the oblique shock waves with large shock angle from other primary cells. The secondary cells of the primary jets from the triple points covered the secondary jet. Interactions of the secondary cells and the secondary jet yielded weak oblique shock waves. The oblieque shock waves suffered Mach reflection and yielded a concaved Mach disk (Riemann wave) accompanied with a reverse flow. In the same time, slip flow surrounding the secondary jet converged towards the line of symmetry. This convergence of the slip flow and the resulting reverse flow might be attributed to the decrease of stagnation pressure in the secondary jet, which was caused from the entropy production due to the oblieque shock wave with large shock angle.

1. Introduction

Underexpanded free jet from a nozzle or a orifice with high pressure ration between resovior and ambient gas yields a cell of isentropic flow, which is surrounded with barrel shock and Mach disk (Riemann wave). The isentropic flow is decelerated through the Riemann

*Present address, ANA, Tokyo

wave and becomes subsonic behind the Mach disk. If the ratio of pressure is small, the barrel shock of the expansion flow from a supersonic nozzle suffers regular reflection and then the supersonic flow still holds in the downstream. Free expansion flow from multi-nozzles is seen in the exhaust flow from an ascending rocket at high altitude. Recently, Venkatapathy and Feiereisen[1] have obtained a numerical solution of the Navier-Stokes equation applied to such an exhaust flow from multi-nozzles. It is also well known that a weak reverse flow towards the base of rocket takes place due to the interaction of nozzle-jets.

Experimental results[2] showed that interaction of paralell jets issued from sonic orifices yielded an intensive secondary jet expanding in the duct made of oblieque shock waves. Since one of the symmetric plane can be regarded as a smooth flat plate, this secondary jet can be caused from a plume impingement on the plate. Numerical simulation of Ivanov and Kraiko[3] yielded such a feature of plume impingement. Interaction of free jets more than three may yield a flow field enclosed by the oblieque shock waves. The resulting secondary jet may be quite different from the free jets from orifices. Increasing the number of orifices, we will have a flow field of free jet from a ring-like orifice. Since the flow field behind a semisphere held in the hypersonic flow is similar to such a expansion flow, study of the abovementioned bounded flow must be significant.

Present authors are interested in the abovementioned internal flow bounded by free jets and intend to know the details of the flow field of jets interaction. Since the flow field of free jets from multi-orifices is not surrounded with any solid walls, the roll of viscosity may be less important for the prediction of this flow field. Therefore, numerical simulation is carried out within the framework of the Euler equation. Present numerical simulation is directed to grasp the overall structure of the flow field rather than the details of multi-reflection of shock waves. Since the Pieceweise Linear Method (PLM)[4] is substantially a sort of TVD scheme and has yielded satisfactory results for the numerical analysis of free jet[5]. We employ this method in the present numerical simulation. For numerical simplicity, we use square orifices instead of circular orifice. Results of numerical simulation of free jets from atmost four square orifices are presented in this report.

2. Numerical Analysis

A. Basic Equation

Flow field of free jets from multi-orifices is complex, involving interaction between the primary jets, interaction between the secondary jet and the second cells of the primary jets, and impingement of a reverse flow on the secondary jet. In order to describe the overall flow field, the three-dimensional Euler equation is employed. The governing equation is written in the conservative form;

$$\frac{\partial \mathbf{U}}{\partial t}+\frac{\partial \mathbf{F}(\mathbf{U})}{\partial x}+\frac{\partial \mathbf{G}(\mathbf{U})}{\partial y}+\frac{\partial \mathbf{H}(\mathbf{U})}{\partial z}=0 \tag{1}$$

where

$$\mathbf{U}=\begin{pmatrix}\rho\\ \rho u\\ \rho v\\ \rho w\\ e\end{pmatrix},\quad \mathbf{F}=\begin{pmatrix}\rho u\\ \rho u^2+p\\ \rho uv\\ \rho uw\\ u(e+p)\end{pmatrix},\quad \mathbf{G}=\begin{pmatrix}\rho v\\ \rho uv\\ \rho v^2+p\\ \rho vw\\ v(e+p)\end{pmatrix},\quad \mathbf{H}=\begin{pmatrix}\rho w\\ \rho uw\\ \rho vw\\ \rho w^2+p\\ w(e+p)\end{pmatrix} \tag{2}$$

Notations used in the equation are conventional ones. The ratio of specific heats γ is considered to be constant, $\gamma = 1.4$.

B. Piecewise Linear Method

In Godunov's method (see Holt[6]) unsteady flow is resolved to the Riemann problems (shock tube problems) of many cells where the boundaries of each cell are regarded as membranes in the shock tube. Godunov's method is able to improve, approximating flow properties in the cell by linear functions[7]. This improved method is called as Piecewise Linear Method (PLM), which retains higher order accuracy in space except shock waves where the accuracy is degraded to first order. Using the time splitting method[7], PLM holds second order accuracy in time. For the three-dimensional problem Strang's[8] time splitting method is introduced so as to retain the second order accuracy in time. Colella and Woodward[9] extended this idea further and proposed Piecewise Parabolic Method (PPM). Speed up of the Godunov's method was done by Colella[10] and Colella and Glaz[11] with the aid of an approximate Riemann solver. On the other hand Gottlieb and Groth[12] proposed a new iterative procedure without approximate solvers. Since the results of the PPM[13] have shown no remarkable improvement to the PLM, we employ the PLM in the present simulation of free jets from multi-orifices.

Introducing the time splitting method proposed by Strang[8], the basic equation (1) can be splitted to three one-dimensional partial difference equations,

$$\frac{\partial \mathbf{U}}{\partial t}+\frac{\partial \mathbf{F}}{\partial x}=0 \tag{3}$$

$$\frac{\partial \mathbf{U}}{\partial t}+\frac{\partial \mathbf{G}}{\partial y}=0 \tag{4}$$

$$\frac{\partial \mathbf{U}}{\partial t}+\frac{\partial \mathbf{H}}{\partial z}=0 \tag{5}$$

If Eqs. (3) to (5) yields

$$\mathbf{U}^{n+1}=S^x_{\Delta t}\mathbf{U}^n \tag{6}$$

$$\mathbf{U}^{n+1}=S^y_{\Delta t}\mathbf{U}^n \tag{7}$$

$$\mathbf{U}^{n+1}=S^z_{\Delta t}\mathbf{U}^n \tag{8}$$

solution of Eq. (1) can be given by

$$\mathbf{U}^{n+1}=S_{\Delta t}\mathbf{U}^n,$$

where $\mathbf{U}^n$ and $\mathbf{U}^{n+1}$ are respectively the solution of Eq. (1) at $t = t^n$ and $t = t^{n+1}$ $(= t^n + \Delta t)$. The difference operator $S_{\Delta t}$ is expressed as

$$S_{\Delta t} = S^x_{\frac{\Delta t}{2}} S^y_{\frac{\Delta t}{2}} S^z_{\Delta t} S^y_{\frac{\Delta t}{2}} S^x_{\frac{\Delta t}{2}} \tag{9}$$

where the operator $S_{\Delta t}$ retains the second order accuracy.

Employing the time splitting method, the three-dimensional problem is thus reduced to the one-dimensional problems. The numerical simulation proceeds through the following five steps; we assume that we know all U^n:

1. Obtain the distributions of p, ρ, and u in the cell of simulation.
2. Obtain the value of p, ρ, and u at the boundaries (right and left) of the cell at $\Delta t/2$.
3. Solve the Riemann problem, employing the p, ρ, and u at the both side of the boundary (this boundary is equivalent to the membrane of shock tube) as the initial conditions and obtain the values of p, ρ, and u after breakdown of the membrane.
4. Evaluate $\mathbf{F}^{t+\Delta t/2}$ at the boundary.
5. Obtain $\mathbf{U}_c^{t+\Delta t}$, using the difference equation

$$\mathbf{U}_c^{t+\Delta t} = \mathbf{U}_c^t + \frac{\Delta t}{\Delta x_j}(\mathbf{F}_{bl} - \mathbf{F}_{br})$$

where the subscripts c, bl, and br denote the center of the cell, the left boundary, and the right boundary, respectively.

For the sake of time saving Riemann problem is solved employing the Rankine-Hugoniot relation solely[14]. Details of the numerical procedure are shown in reference 4. In employing the program code we need to improved the original code so that we may evaluate any reverse flows. Using the abovementioned schems, the governing equations are solved numerically under appropriate boundary conditions described below.

C. *Flow Field of Simulation and Boundary Conditions*

Flow fields from single orifice, from two orifices, and from four orifices have two or more planes of symmetry. So, one fourth of the flow field cut by these planes shown in Fig. 1 is used for the numerical simulation. The origin of the coordinates is set in the cente of an orifice or orifices, i.e., the point of intersection of the two planes of symmetry and the plane including the orifices. We take the x axis along the line of intersection of two planes of symmetry. The remaining two lines of intersection among the three planes are taken as y and z axes, respectively. The width of the orifice w is devided into eight meshs ($\mathrm{w} = 8\Delta y$) for the cases of free jet from single orifice and from two orifices. The domain of simulation is taken as $45\Delta\mathrm{x}\times45\Delta\mathrm{y}\times\Delta\mathrm{z}$ where we set $\Delta\mathrm{x} = 2\Delta\mathrm{y} = 2\Delta\mathrm{z}$. In the case of free jets from four orifices the width of the orifice is approximated by 6 meshs and the domain of simulation is taken as $50\Delta\mathrm{x}\times45\Delta\mathrm{y}\times45\Delta\mathrm{z}$. Distance of side to side of orifices is taken as $1\times\mathrm{H}$, the width of the orifice.

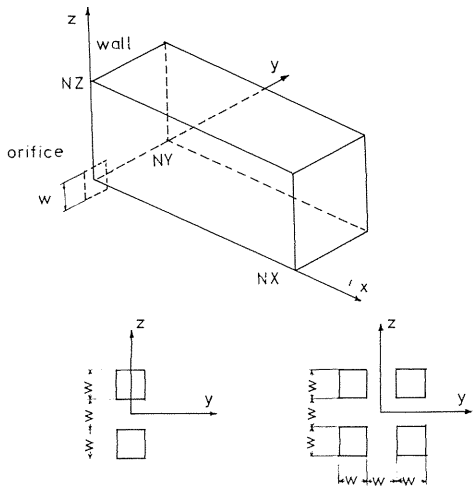

Fig. 1 Coodinates System and caluculation region.

The region of calculation is at first filled with the gas of ambient conditions of the expansion chamber. Sonic conditions are applied to the orifice (or orifices) and then gas issues from the orifice or orifices with sonic conditions. The boundary conditions at the surface including the orifice (or orifices) (x = 0) are given as specular reflection except for the orifice (or orifices). Same boundary conditions are given for the planes of symmetry; y = 0 for the case of two orifices and y = 0 and z = 0 for the case of four orifices, respectively. At the circumference the initial conditions of ambient gas are used as the boundary conditions. At the downstream end of the calculation region, we employ the conditions of zero-gradient of flow parameter. Using the Courant's number 0.8, i.e., $|\Delta x/(u+c)_{max}| < 0.8$, calculation has been carried out over 4000 steps. The residual of density ϵ defined by

$$\epsilon_i = \sum_{i=1}^{N} |\rho_i - \rho_{i-1}|/N,$$

where N denote the total number of cells used for the calculation, became $O(10^{-4})$.

3. Results and Discussion

A. *Results of Free Jet from Single Square Orifice*

Results of numerical simulation are shown in Figs. 2 and 3 for the case of $p_0/p_\infty = 50$. Density contours (left) and velocity vectors (right) in the symmetric plane, z = 0 (upper) and in the diagonal plane, y = z (lower) are shown in Fig. 2, respectively. Density contours in the cross sections perpendicular to the x axis are shown in Fig. 3. An increment of contour is taken as $0.01\rho^*$, where ρ^* denotes sonic condition. As shown in Fig. 3, a side of the orifice changes to a corner and a corner of the orifice changes to a side of the cross section, respectively. The cross section of the free jet seems to be rotated just 90 degrees as the expansion proceeds. The free jet from a square orifice accompanys with four fins developing along the planes of symmetry, i.e., the x-y plane at z = 0 and x-z plane at y = 0. The outermost contour of the fins are, however, incorrectly drawn. Features of these fins will be discussed later.

As a whole, present results are close to the previous results otained by Teshima[5]. Density contours downstream of the Mach disk in Fig. 3 ($x \geq 6$) show a rotated square form with thick fins as are shown in the experimental results[15]. But the previous results otained by Teshima[5] showed a recovary to the original square form with fins. This may imply that Teshima's results showed a rapid convergence (focussing) of the free jet behind the Mach disk.

Plateaus of density shown in Fig. 4 (x/w = 10 and 11) are well corresponding to the luminous parts of the fins in the photographs of experiments[15].

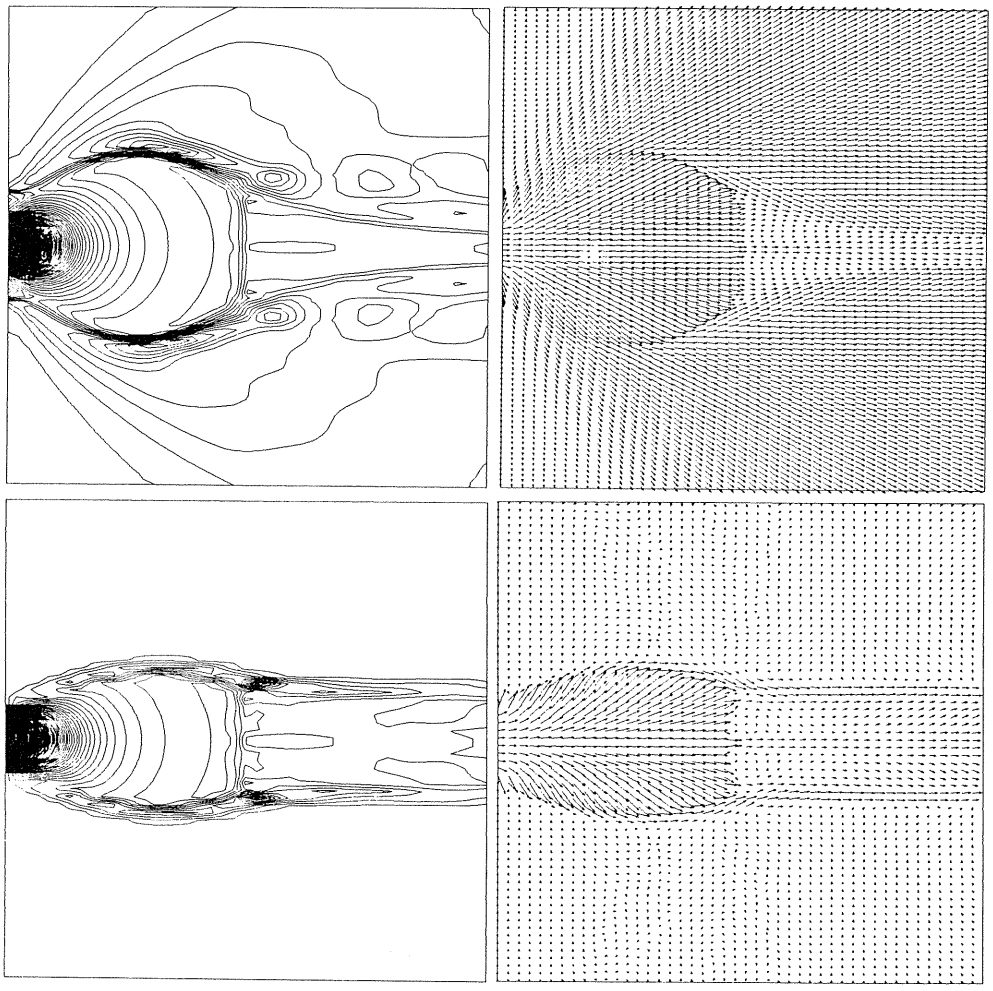

Fig. 2 Density contour (left) and velocity vectors (right) in the symmetric plane (z = 0) (upper) and in the orthogonal plane (y = z) (lower) for single orifice.

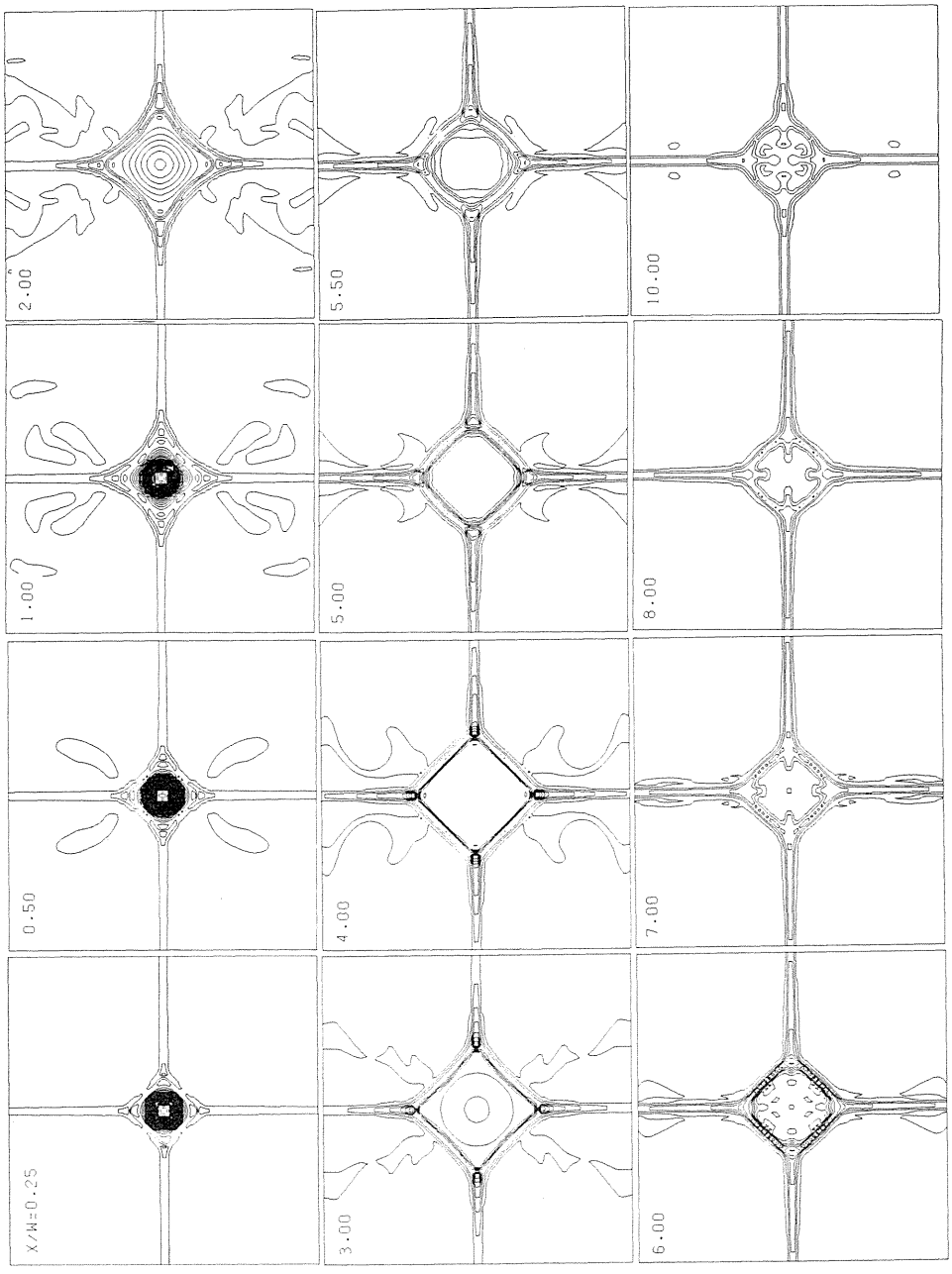

Fig. 3 Density contour in the cross sections at different location on the x axis for single orifice.

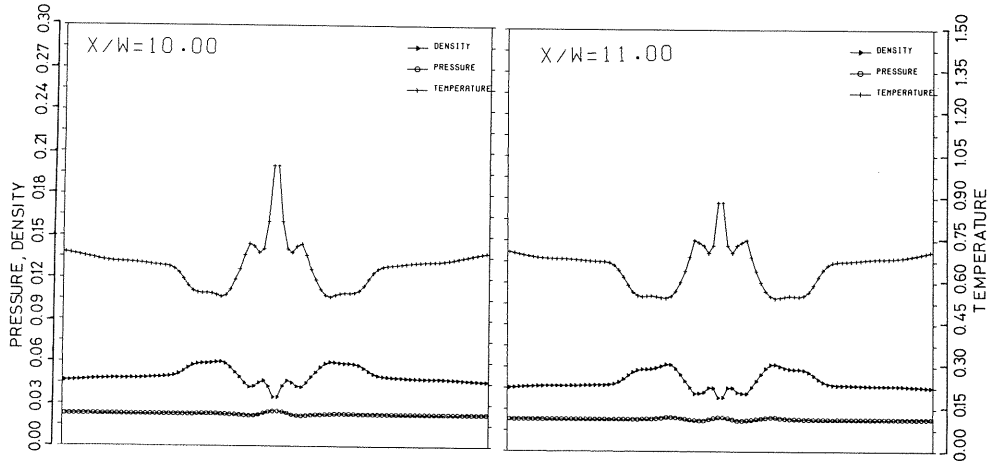

Fig. 4 Distributions of pressure, temperature, and density along the line in the cross section in Fig. 3 and y = 0 for single orifices.

B. *Results of Free Jets from Two Square Orifices*

Results of free jets from two square orifices are shown in Figs. 5 and 6 for the case of $p_0/p_\infty = 50$. Density contours (left) and velocity vectors (right) in the symmetric planes, z = 0 (upper) and y = 0 (lower) are respectively shown in Fig. 5. Density contours in the cross sections perpendicular to the x axis are shown in Fig. 6 where the increment of contour is taken as $0.01\rho^*$. As shown in Fig. 5 (left and under), interaction of two free jets yields oblieque shock waves. These shock waves are also seen in Fig. 6 (x/w = 1.5 and x/w = 2.0). Recompressed gas between the oblieque shock waves is expanding in the symmetric plane, z-y plane, so that the primary free jets are enlarged and unified as shown in Fig. 5 (left). Pressure, density, and temperature distributions along the line of intersection of the symmetric plane y = 0 and the cross section shown in Fig. 6 are presented in Fig. 7. These distributions are useful to understand the shock interactions taken place in the present simulation. The pressure distributions show that the abovementioned oblieque shock waves fade out for $x > 5$. Finally Mach waves impinges on the outer shock waves, yielding weak slip slows (see Fig. 5 (left)). The free jets expansion from two orifices may be in some sense close to the expansion from a rectangular orifice with the aspect ratio, $L/w \approx 3$ or so where L denotes the length of the longer side of the rectangular. Present results show a convergence of free jet toward the symmetric plane z = 0. Consequently, reexpansion of gas in the direction of y axis results in formation of cells of weak diamod shock waves (see Fig. 6 ($x/w \geq 6$)). The experimental results of Teshima[15] presented such cells for the case of L/w = 5 and $p_0/p_\infty = 100$.

As mentioned above, Teshima[15] found that free jet expanding from a rectangular sonic orifice has fins. Since rarefaction waves reflected from quiecent gas changes to shock waves, free jet from the square orifice (or orifices) is bounded with a shock wave having a (almost) square cross section. In the vicinity of the symmetric plane, certain overshoots of density and/or pressure take place due to the impingement of the shock waves which enclose the free jet as shown in Fig. 7. The overshoot of density yields a slip flow outside of the surrounding shock wave (Fig. 7, x/w = 2), while the overshoot of pressure and density yields reexpansion

of gas in the direction of z axis accompanied with a slip flow (Fig. 7, x/w = 4). Luminous fins shown in the experiment may be such a expansion fan. So long as the velocity component perpendiculat to the symmetric plane is small, the slip flow and the reexpansion of gas take place in the plane of symmetry.

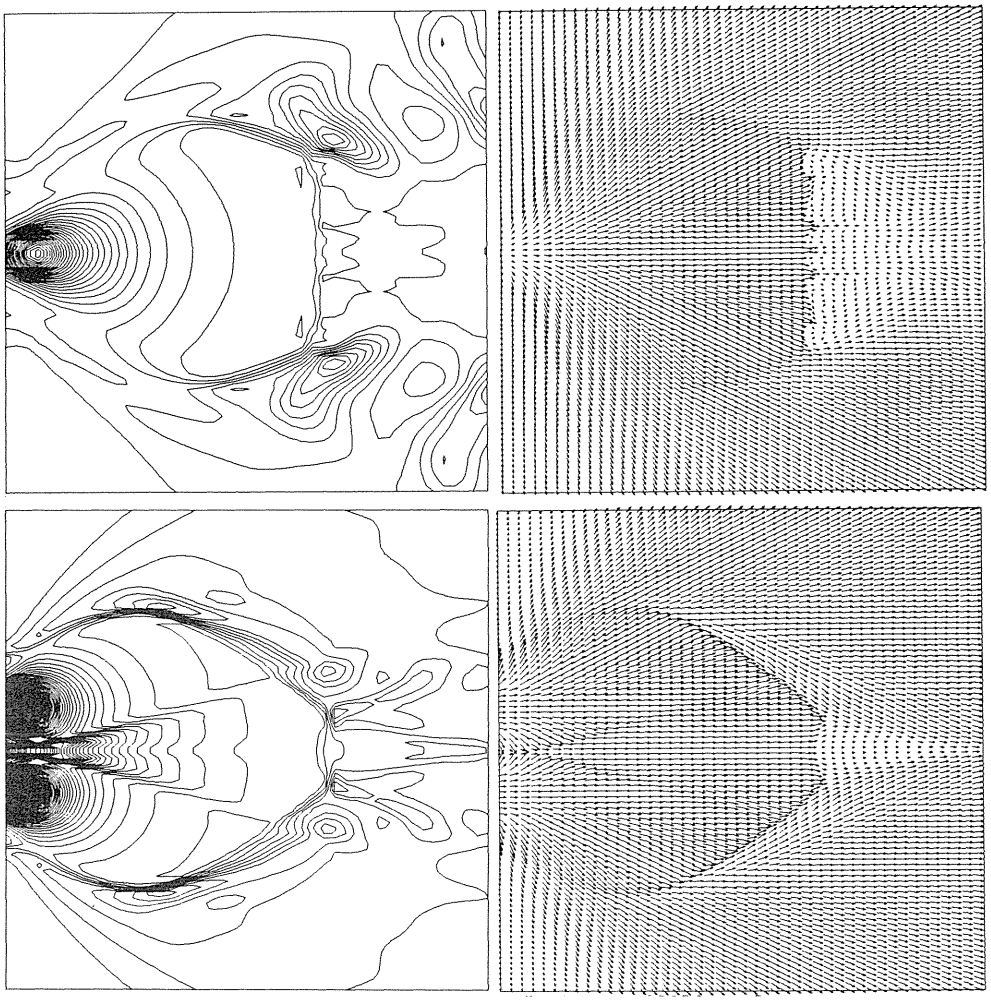

Fig. 5 Density contour (left) and velocity vectors (right) in the symmetric planes, z = 0 (upper) and y = 0 (lower) for two orifices.

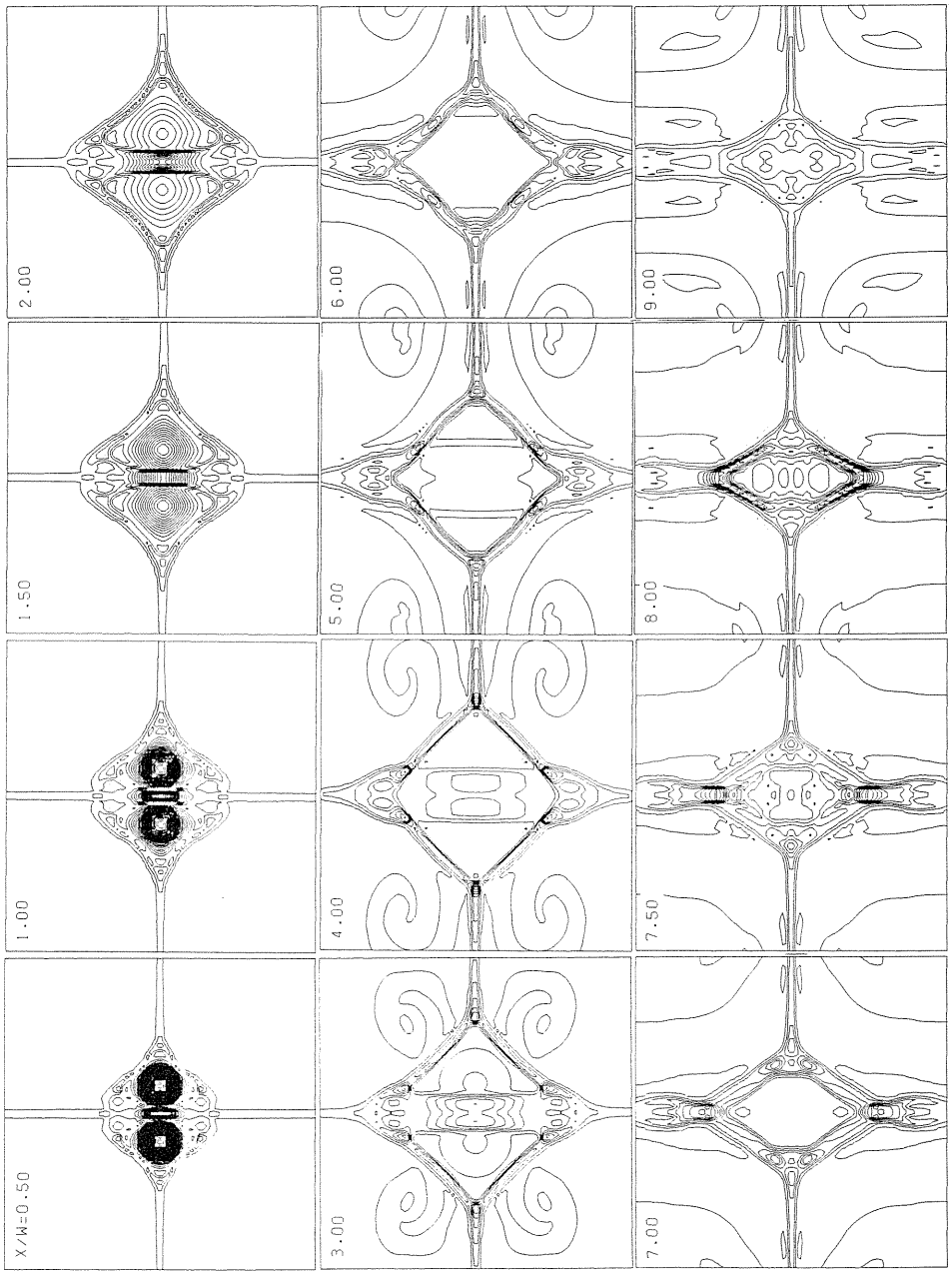

Fig. 6 Density contour in the cross sections at different location on the x axis for two orifices.

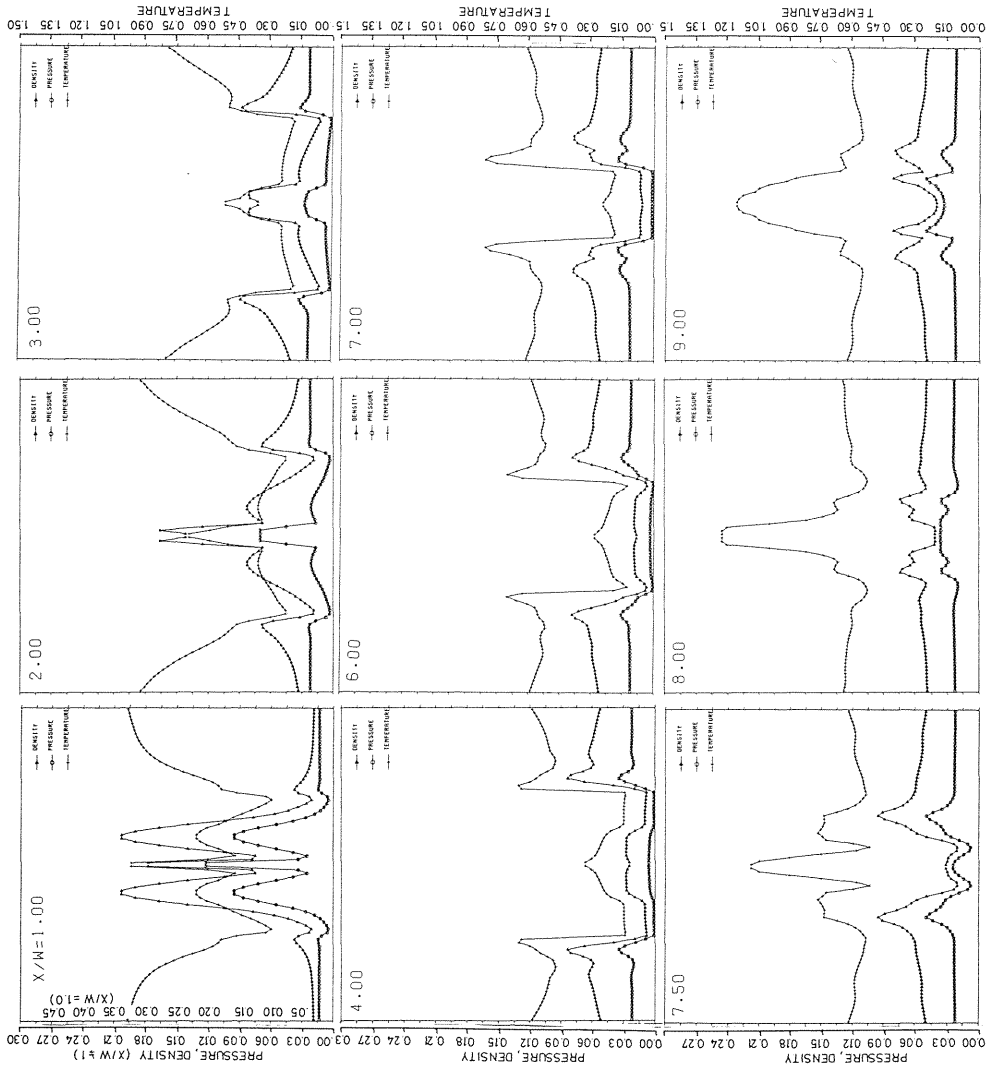

Fig. 7 Distributions of pressure, temperature, and density along the line in the cross section in Fig. 5 and y = 0 for two orifices.

C. *Results of Free Jets from Four Orifices*

Results of free jets from four rectangular orifices are shown in Figs. 8 and 9 for the case of $p_0/p_\infty = 50$. Density contours (left) and velocity vectors (right) in the symmetric planes, z = 0 (upper) and in the diagonal plane y = z (lower) are respectively shown in Fig. 8. Density contours in the cross sections perpendicular to the x axis are shown in Fig. 9, where the increment of contour is taken as $0.01\rho^*$. As shown in Fig. 8 (left and under), interaction of four free jets yields steep oblieque shock waves having a shock angle of 30 degrees. It is worth

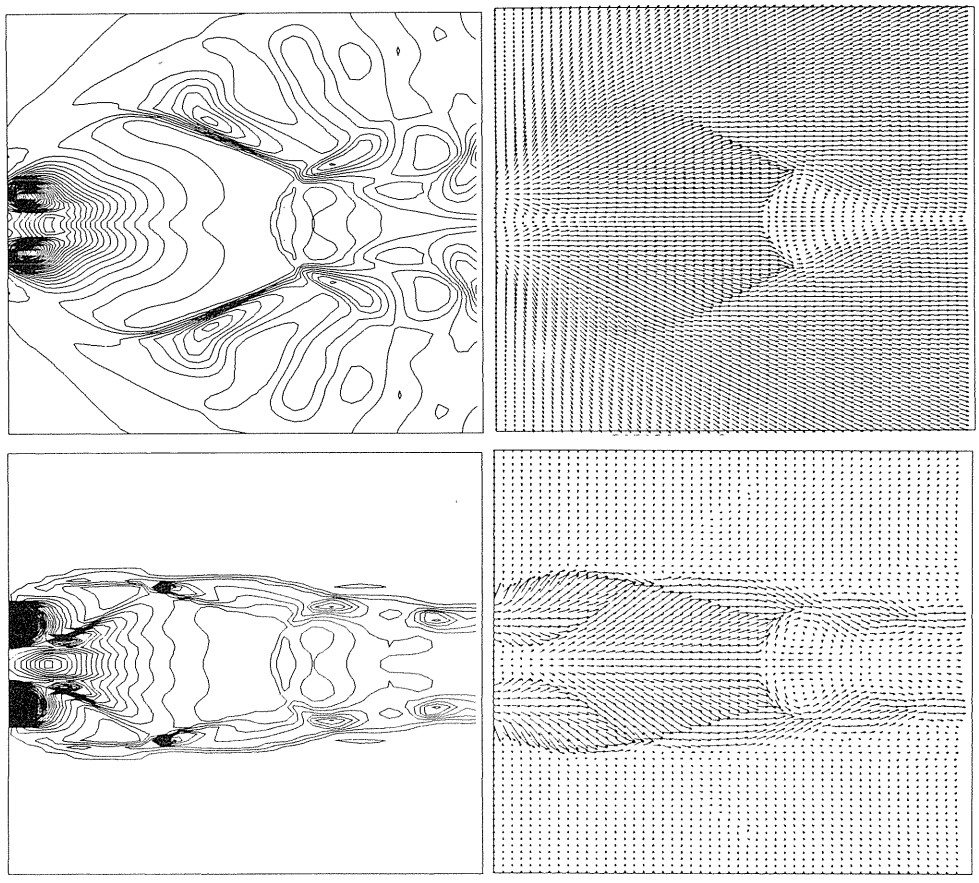

Fig. 8 Density contour (left) and velocity vectors (right) in the symmetric plane, z = 0 (upper) and in the orthogonal plane y = z (lower) for four orifices.

noting that this angle is about twice of the shock angle shown in Fig. 5 (left). These shock waves are seen also in Fig. 9 (x/w = 2.0 and x/w = 3.0).

Recompressed gas through the oblieque shock wave is expanding intensively and establishes a cell of secondary jet. The oblieque shock wave impinges on the surrounding shock waves of the primary free jets and then the oblieque shock wave starts to converge. Very weak secondary cells of the primary free jets and thick slip flow (jet boundary) bound this secondary jet. The converging oblieque shock wave impinges each other, yielding reflected shock waves and a curved Mach disk (Fig. 8). Through the reflected oblieque shock wave, the slip flow is turned up but the flow eventually converges on the line of symmetry: This may be attributed to the fact that the stagnation pressure of the secondary jet is lower than that of the primary jet. Consequently a stagnation point emerges in the downstream of the Mach disk and then reverse flow takes place as shown in Fig. 7.

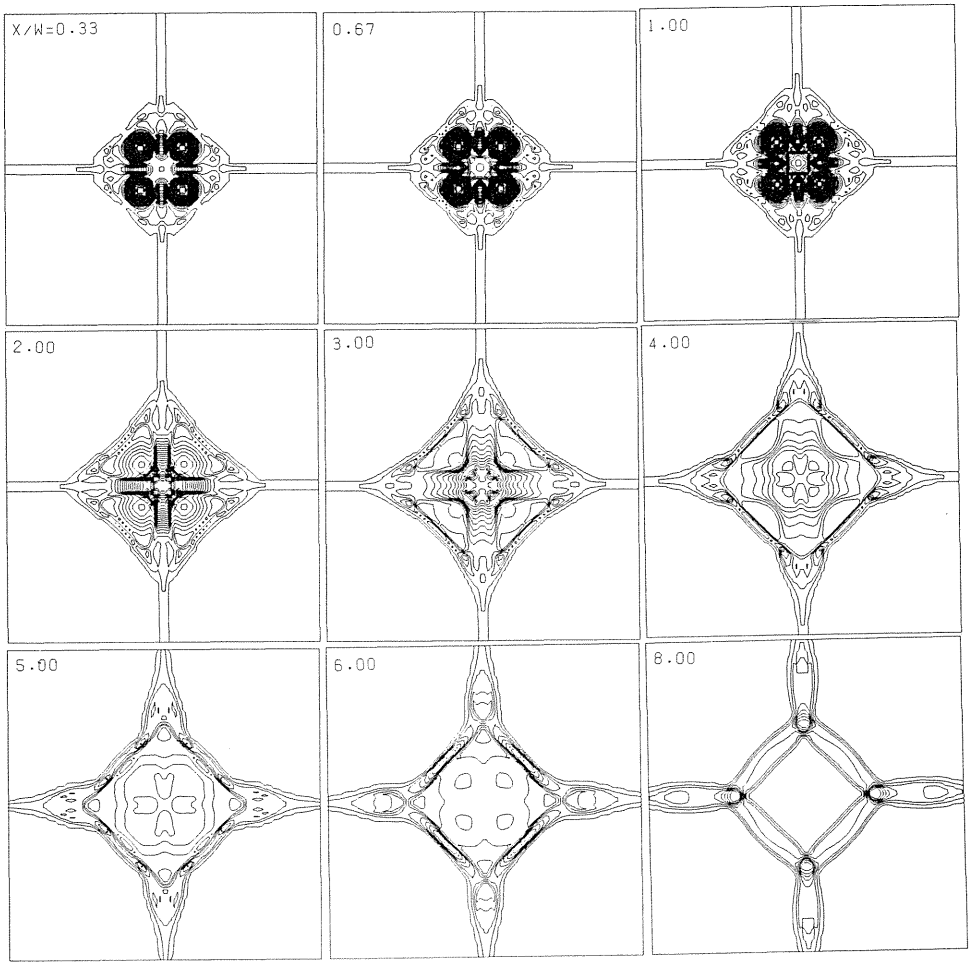

Fig. 9a Density contour in the cross sections at different location on the x axis for four orifices: upstream of the Mach disk.

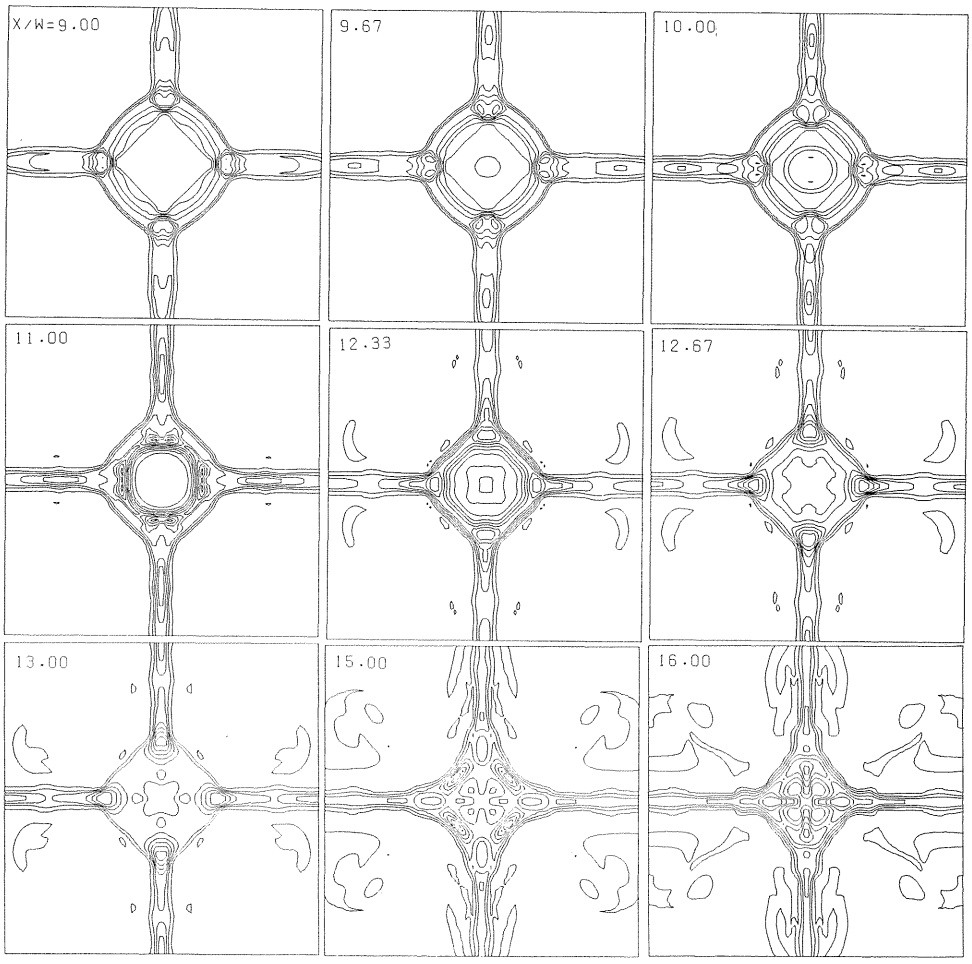

Fig. 9b Density contour in the cross sections at different location on the x axis for four orifices: downstream of the Mach disk.

Distributions of velocity and Mach number along the line of symmetry (the line of intersection of symmetric planes) are shown in Fig. 10. Whether or not such a reverse flow takes place may be dependent upon the difference of the stagnation pressure between the primary jet and the secondary jet. It should be mentioned that the present results show somewhat higher stagnation temperature than the reservoir temperature at the stagnation point downstream of the Mach disk. This must be partly dependent upon the accuracy of the numerical method but in the same time the obtained results can express certain unsteady motion of the free jet.

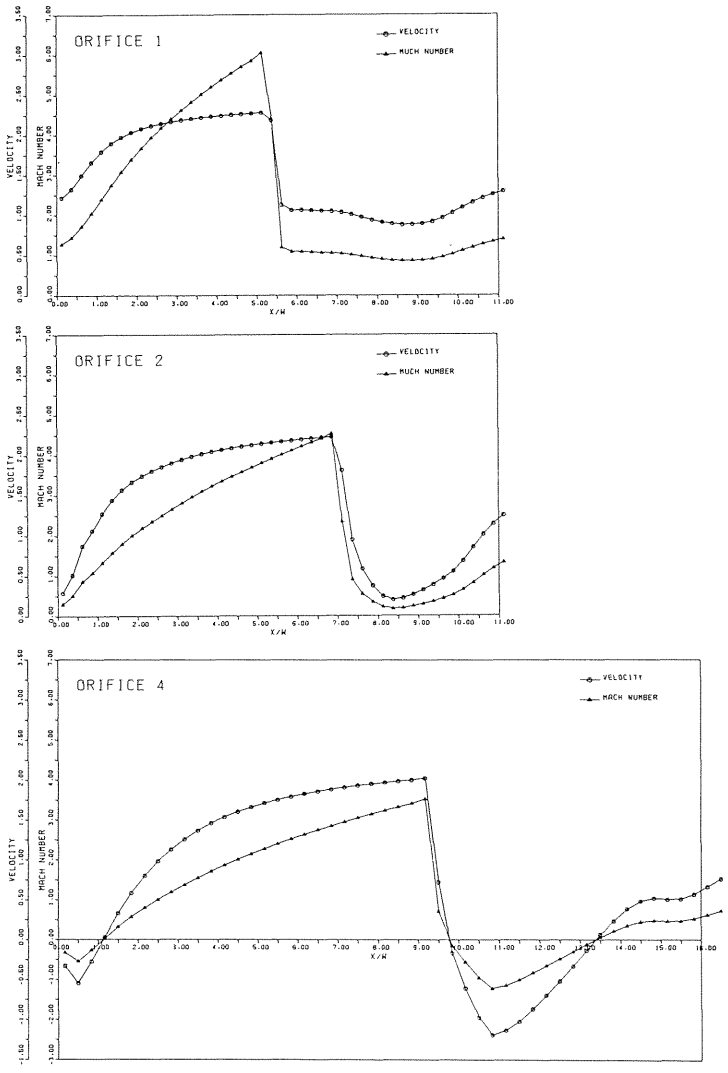

Fig. 10 Distributions of velocity and Mach number along the line symmetry (y = z = 0).

4. Conclusions

Numerical simulations of free jet or jets from single square orifice, from two square orifices, and from four square orifices were carried out using an Euler solver (PLM). Interaction (or impingement) of free jet yielded an intensive secondary jet bounded by oblieque shock waves. Entropy production due to the oblieque shock wave resulted in a decrease of stagnation pressure in the secondary jet. Thick slip flows and vorticities were accordingly induced. In the case of free jets from four orifices, the shock angle of the oblieque shock waves of the

secondary jet was about twice of that of the free jets from two orifices. Consequently, strong convergence of the slip flow that surrounded the secondary jet took place and yielded a concaved Mach disk. Amount of entropy production due to the oblieque shock wave was so much that vorticty had grown up to a reverse flow behind the Mach disk. It may be interesting to study further whether or not such an unsustained reverse flow is substantially steady. More refined numerical method such as Piecewise Parabolic Method and any limitters must be useful for such a further study.

References

1) E. Venkatapathy and W.J. Feiereisen: 3-D plume flow computations with an upwind solver, AIAA-88-3158, pp.1–12 (1988).
2) T. Soga, M. Takanishi and M. Yasuhara: Experimental study of interaction of underexpanded free jets, in *Rarefied Gas Dynamics*, edited by H. Oguchi (Tokyo Univ. Press, Tokyo, 1984), Vol.I, pp.485–492.
3) M. JA. Ivanov and A.N. Kraiko: Numerical simulation of external and internal gasdynamics problem, Acta Astronautica 8, pp.325–335 (1981).
4) K. Teshima and K. Abe: Analysis of axisymmetric flow employing PLM, Rep. Computer Center of Kyoto Univ., Vol.19, No. 3 (1986).
5) K. Teshima: Three-dimensional structure of a supersonic free jet issuing from a rectangular orifice, in *Numerical methods in fluid dynamics II*, edited by M. Yasuhara, H. Daiguji, and K. Oshima (Japan Society of Fluid Dynamics, 1989), pp.993–999.
6) M. Holt: *"Numerical Methods in Fluid Dynamics"*, (Springer-Verlag, 1984) p.28.
7) B.van Leer: Towards the Ultimate Conservative Difference Scheme V.A Second - Order Sequel to Godunov's Method, J. Comput. Phys., Vol.32, pp.101–136 (1979).
8) W.G. Strang: On the Construction and Comparison of Difference Schemes, SIAM J. Numer. Anal., Vol.5, pp.506–517 (1968).
9) P. Colella and P.R. Woodward: The Piecewise Parabolic Method (PPM) for Gas-Dynamical Simulations, J. Comput. Phys., Vol.54, pp.174–201 (1984).
10) P. Colella: A Direct Eulerian MUSCL Scheme for Gas Dynamics, SIAM J. Sci. Stat. Comput., Vol.6, pp.104–117 (1985).
11) P. Colella and H.M. Glaz: Efficient Solution Algorithms for the Riemann Problem for Real Gases, J. Comput. Phys., Vol.59, pp.264–289 (1985).
12) J.J. Gottlieb and C.P.T. Groth: Assessment of Riemann Solvers for Unsteady One-Dimensional Inviscid Flows of Perfect Gases, J. Comput. Phys., Vol.78, pp.437–458 (1988).
13) Y. Kato: Studies on free jets and analysis of high speed flow employing parabolic equation, Master thesis, Dep. Aeronaut. Engng., Nagoya University, 1989.
14) P. Colella: Glimm's Method for Gas Dynamics SIAM J. Sci. Stat. Comput., Vol.3, pp.76–110 (1982).
15) K. Teshima: Three-dimensional characteristics of supersonic jets, in *Rarefied Gas Dynamics*, edited by A.E. Beylich, (VCH Press, Weinheim, 1991), pp.1042–1048.